Symmetry and charge order in Fe_2OBO_3 studied through polarized resonant x-ray diffraction

S. R. Bland,[1] M. Angst,[2] S. Adiga,[2] V. Scagnoli,[3] R. D. Johnson,[1] J. Herrero-Martín,[3] and P. D. Hatton[1]
[1]*Department of Physics, Durham University, Rochester Building, South Road, Durham DH1 3LE, United Kingdom*
[2]*Institut für Festkörperforschung, JCNS, and JARA-FIT, Forschungszentrum Jülich GmbH, D-52425 Jülich, Germany*
[3]*European Synchrotron Radiation Facility, F-38043 Grenoble, France*
(Received 7 May 2010; revised manuscript received 26 July 2010; published 10 September 2010)

Bond valence sum calculations have previously suggested that iron oxyborate exhibits charge order of the Fe ions with integer 2+/3+ valence states. Meanwhile transition metal oxides typically show much smaller, fractional charge disproportionations. Using resonant x-ray diffraction at the iron *K* edge, we find resonant features which are much larger than those ordinarily observed in charge ordered oxides. Simulations were subsequently performed using a cluster-based, monoelectronic code. The nanoscale domain structure prevents precise fitting; nevertheless the simulations confirm the diagonal charge order symmetry, as well as the unusually large charge disproportionation. We have demonstrated the conversion of linearly to nonlinearly polarized light and vice versa through full polarization analysis. Simulations show that this effect principally results from interference between the isotropic and anisotropic scattering terms. This mechanism is likely to account for similar observations in alternative systems.

DOI: 10.1103/PhysRevB.82.115110 PACS number(s): 71.30.+h, 71.28.+d, 75.25.Dk, 71.27.+a

I. INTRODUCTION

The question of whether the phenomenon of charge ordering is driven through electrostatic repulsion (Wigner crystallization[1]) or through electron-lattice coupling (principally cooperative Jahn-Teller distortions[2,3]) has been the subject of considerable interest in recent years. This is particularly true for the case of the perovskite manganites, where a competition between the two phenomena apparently helps determine the charge configuration.[4–6] Iron oxyborate is a fascinating material when addressed in this context, as it appears to show characteristics of a model Wigner system.[7,8]

At high-temperature iron oxyborate is orthorhombic,[7] with space group *Pmcn* (No. 62) and lattice parameters $a=3.1779$ Å, $b=9.3945$ Å, and $c=9.2495$ Å. The structure consists of chains of four octahedra, as shown in Fig. 1, which are linked indefinitely along the *a* axis. In this high-temperature phase, octahedral sites I & IV, and II & III are crystallographically equivalent. Jumps in electrical resistance are apparent at ~340 and ~310 K on cooling, with a hysteretic loop extending over 55 K below the second transition.[9] Mössbauer spectra have indicated that above 270 K there exists an electron hopping component, while below 270 K the fluctuations cease, and the spectra suggest that divalent and trivalent ions are equally distributed over the two crystallographically different sites. Below ~155 K the system magnetically orders, becoming an *L*-type ferrimagnet.[10]

In the charge ordered phase the structure becomes monoclinic with a maximum monoclinic angle of ~90.2° at ~190 K, and a doubled *a* axis supercell, as first suggested by Attfield *et al.*[7,8] The original proposed charge ordered structure is shown in Fig. 2(a). Local spin density approximation plus *U* (LSDA+*U*) calculations have predicted the same charge ordered structure as the Attfield configuration, as well as correctly determining the sizes of the ferrimagnetic moment and the band gap.[11] These calculations have also predicted a total 3*d* band charge separation of $0.34e^-$ between the formally Fe^{2+} and Fe^{3+} sites. Generalized gradient approximation plus *U* (GGA+*U*) calculations with structural optimization have also confirmed the diagonal charge configuration as the favorable solution, although an alternative zigzag configuration has been found, which is only slightly less energetically favorable.[9]

Recently the growth of single crystals of Fe_2OBO_3 has become possible, widening the scope for new diffraction studies. Charge order reflections have been identified at low temperatures, at a wave vector of $(h+\frac{1}{2},k,l)$, confirming the doubled *a* axis of the supercell.[12] Further studies have identified that the commensurate (CM) charge order only appears at ~270 K on cooling, above which incommensurate (ICM) reflections are visible at $(h+\frac{1}{2},k,l\pm\tau)$ positions. Here, τ is temperature dependent and increases from 0.25 at ~270 K to 0.4 at 340 K. Above this temperature the reflections be-

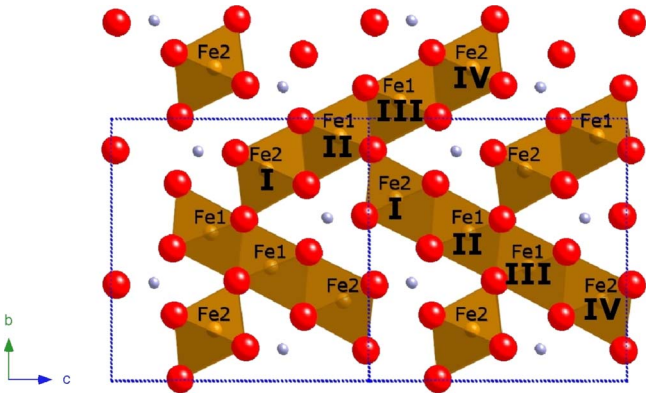

FIG. 1. (Color online) Crystal structure of iron oxyborate, Fe_2OBO_3. The iron, oxygen, and boron atoms are shown as brown (inside polyhedra), red (large), and silver (small) spheres, respectively. The blue dashed lines represent the high-temperature unit cell. Chains of four octahedra are linked in an edge sharing network, containing two crystallographically distinct sites. Each chain continues infinitely along the *a* axis.

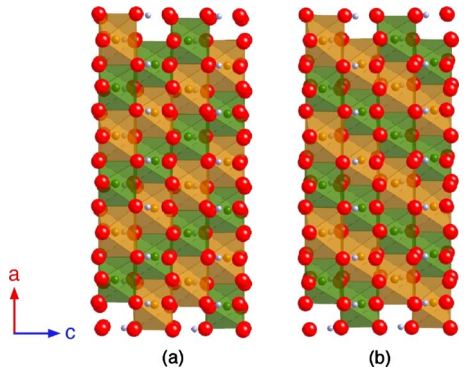

FIG. 2. (Color online) A single iron chain, with the (a) up and (b) down diagonal charge ordered structures. The orange sites are Fe^{2+} while the green sites are Fe^{3+}.

come significantly broader and only short-range correlation exists.[9]

Despite now being able to observe the charge order reflections, confirmation of the charge configuration in the commensurate phase has still proven difficult. The problem arises due to the presence of oppositely distorted charge domains within the crystal: the so-called diagonal *up* and *down* structures shown in Figs. 2(a) and 2(b). As a result of the nanoscale domain[7] twinning, only the average structure has been solved.[12] However, this average structure does include some fascinating results, as bond valence sum (BVS) calculations indicate that the system possesses close to true Fe^{2+}/Fe^{3+} integer valences. Such a large charge disproportionation is unusual, as most charge ordered transition metal oxides have typically shown much smaller, fractional charge separations.[13–18]

Resonant x-ray diffraction (RXD) has become an increasingly important technique in studying charge order due to its extreme sensitivity to the local electronic environment of specific ions. How such a large charge disproportionation will affect the resonance is therefore of key interest to the field. By performing a comprehensive RXD experiment, including simulation of the spectra and full polarization analysis,[19,20] we have confirmed the diagonal charge ordered structure, and the large disproportionation. We have also demonstrated the conversion of linearly to nonlinearly polarized light. Unlike previous reports of such a phenomenon,[20,21] this effect appears to principally result from interference between isotropic and anisotropic components.

II. EXPERIMENTAL TECHNIQUE

The sample was prepared using the flux growth technique,[12] producing Fe_2OBO_3 crystals in the form of long needles, approximately 0.2 mm wide and 0.1 mm thick. The crystal was extended along the *a* axis, with an exposed *c* axis normal, natural facet. The experiments were principally carried out on ID20 (Ref. 22) at the ESRF, using a 4+1 circle diffractometer in vertical scattering geometry, although additional measurements were carried out on BM28 (XMaS) (Ref. 23) at the ESRF.

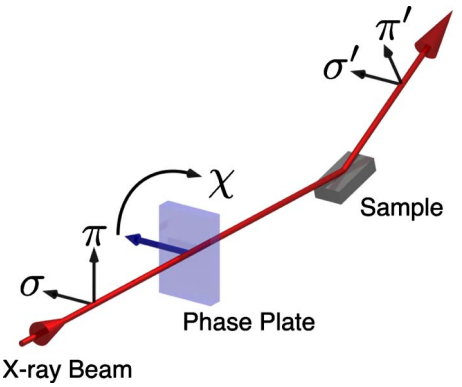

FIG. 3. (Color online) Experimental layout showing the σ and π polarization channels and the sense of the phase plate rotation, χ.

An MgO (2, 2, 2) analyzer was used for postscatter polarization analysis and was found to operate with a maximum channel leakthrough of approximately 0.6%. A diamond phase plate was used to provide any arbitrary incident polarization state required.[24] The experimental geometry is shown in Fig. 3, indicating the definition of the σ and π polarization channels. However, for arbitrary polarization states it is convenient to use the self-normalized Stokes' parameters,[25]

$$P_1 = \frac{(I_{\sigma'} - I_{\pi'})}{I_{0'}}, \tag{1}$$

$$P_2 = \frac{(I_{+45^\circ{}'} - I_{-45^\circ{}'})}{I_{0'}}, \tag{2}$$

$$P_3 = \frac{(I_{\circlearrowright'} - I_{\circlearrowleft'})}{I_{0'}}, \tag{3}$$

where $I_{0'}$ represents the total scattered intensity, and $I_{\sigma'}$ and $I_{\pi'}$ represent the intensities of the scattered σ' and π' channels. $I_{+45^\circ{}'}$ and $I_{-45^\circ{}'}$ represent the intensities of the scattered channels intermediate between σ' and π' while $I_{\circlearrowright'}$ and $I_{\circlearrowleft'}$ represent the scattered intensities in the right and left circularly polarized channels, respectively. Due to the self-normalization we have

$$P_1^2 + P_2^2 + P_3^2 \leq 1, \tag{4}$$

where equality holds for a perfectly polarized beam. We are unable to directly measure the circularly polarized components to find P_3, and so instead we use the square of its upper limit,

$$\text{pseudo-}P_3 = 1 - P_1^2 - P_2^2, \tag{5}$$

thus producing a parameter for all nonlinearly polarized components, i.e., circular polarized and any potential unpolarized components.

III. RESULTS

After aligning the crystal, the sample was rapidly cooled to a base temperature of ≈20 K, before warming to 220 K,

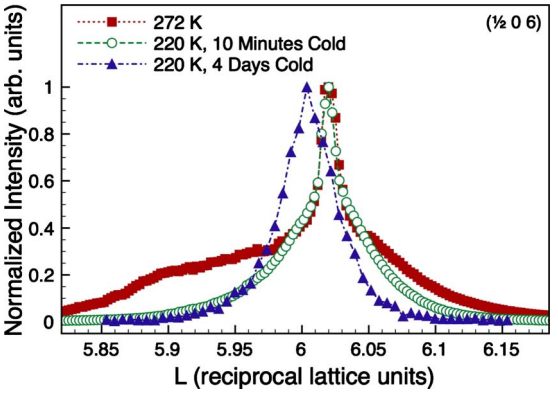

FIG. 4. (Color online) Scans along the L direction for the $(\frac{1}{2},0,6)$ reflection in the σ-σ' channel using an energy of 7.123 keV (on-resonance). The scan at 272 K was measured on cooling from the high-temperature phase, after cooling at a rate of 0.4 K/min. The scan at 220 K was measured after further cooling at the same rate. The final scan was measured after holding the sample at 220 K for 4 days.

above the magnetic transition. However, it quickly became apparent that the rapid cooling had frozen in incommensurate components and resulted in very broad commensurate reflections. The sample was then rewarmed above the hysteretic region and cooled to 220 K at a rate of 0.4 K/min. This slow cooling resulted in a significantly better result, with much sharper commensurate features, and none of the $\pm\tau$ reflections being visible at 220 K. As can be seen in Fig. 4, when the commensurate charge order initially forms it is poorly correlated along the L axis, with well correlated regions condensing out upon further cooling. However, as the structural dynamics are greatly reduced at low temperatures, the development of large correlated regions takes a significant amount of time. After several days of being cold, the diffuse background had disappeared and the reflection had become truly commensurate.

Several other reflections were measured after being held at 220 K for several days, for which the correlation lengths are shown in Table I. The (0, 0, 6) Bragg and forbidden (0, 0, 7) reflections were well correlated along the c axis. This is not surprising as the (0, 0, 7) reflection is expected to be an E1-E1 quadrupolar anisotropy of the tensor of susceptibility [ATS (Ref. 26) or Templeton-Templeton[27]] reflection which is also allowed in the high-temperature phase. Scans along the K direction for the (0, 0, 6) and (0, 0, 7) reflections revealed the sample to have rather poor crystallinity along the b direction, as the reflections consisted of many sharp features.

TABLE I. Correlation lengths of several reflections measured along the c axis at 220 K.

Reflection	Energy (keV)	Correlation length (Å)
(0, 0, 6)	7.123	3387 ± 28
(0, 0, 7)	7.123	1581 ± 55
$(\frac{1}{2},0,6)$	7.123	79 ± 2

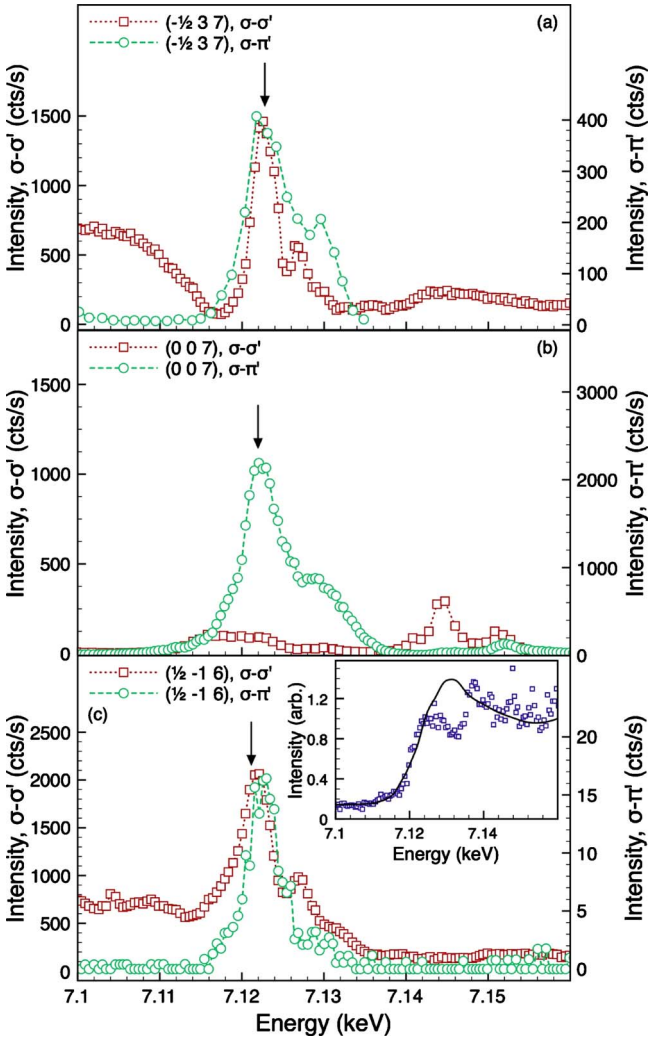

FIG. 5. (Color online) Energy scans of several reflections, measured at fixed wave vector at 220 K. The arrows mark the resonant energies at which full linear polarization analysis was undertaken. Full linear polarization analysis was also undertaken well below the absorption edge for (a) and (c). Inset. The measured (symbols) and simulated (solid line) fluorescence spectrum used for energy calibration.

Numerous $(h+\frac{1}{2},k,l)$ reflections were surveyed and their energy spectra measured, with pronounced energy resonances present in the majority of cases. Some typical spectra are displayed in Fig. 5. We emphasize that these resonances, and those which follow, have not been enhanced through absorption corrections. In addition the $(\frac{1}{2},0,6)$, $(-\frac{1}{2},4,7)$, $(\frac{1}{2},-1,7)$, $(-\frac{1}{2},2,7)$, $(-\frac{1}{2},3,6)$, $(-\frac{1}{2},3,7)$, $(-\frac{3}{2},1,6)$, $(\frac{1}{2},0,7)$, and $(-\frac{3}{2},2,6)$ reflections were also collected. All energy scans were conducted in both the σ-σ' and σ-π' channels, and repeated at an offset azimuthal position in order to confirm that none of the features at the absorption edge originated from multiple scattering.[28]

The temperature dependence of the charge order reflections was studied on the XMaS beamline. The slightly incommensurate nature of the reflections is again clear from the $(-\frac{1}{2},3,7)$ reflection shown in Fig. 6(a). From this figure, we also see a surprisingly large difference between the re-

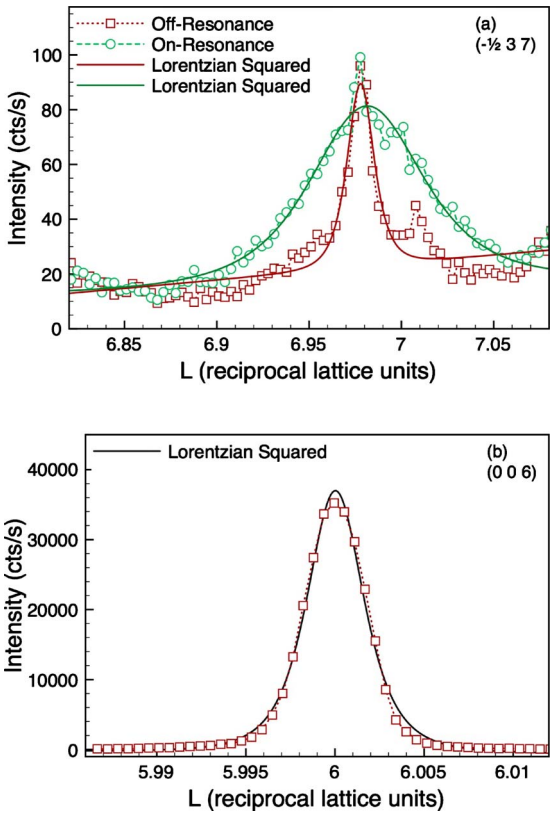

FIG. 6. (Color online) Scans along the L direction for (a) the $(-\frac{1}{2},3,7)$ reflection and (b) the (0, 0, 6) Bragg reflection in the σ-σ' channel measured at 220 K. The former reflection was measured at 7.070 keV (off-resonance) and 7.123 keV (on-resonance).

flection measured on- and off-resonance. The widths associated with the curves fitted to Fig. 6(a) are given in Table II. Of course there is often a broadening of reflections across an absorption edge due to the reduction in the penetration depth of the x-rays. In this case we expect the attenuation length below and above the edge to be 33 μm and 5 μm, respectively. This is three orders of magnitude greater than the correlation lengths reported in Table II, and therefore we believe that the observed increase in width cannot be solely explained as being due to the differences in the scattering volume probed. The broadening on-resonance could be the result of one of two phenomena: either the charge order that we are sensitive to on-resonance is less correlated than the structural distortion or the charge order is less correlated within the first 5 μm of the surface than it is within the bulk of the crystal. As the crystal distortions and the charge order are fundamentally linked, it is highly unlikely that the two phenomena could have such different correlation lengths: in-

TABLE II. Correlation lengths measured on- and off-resonance along the c axis at 220 K.

Reflection	Energy (keV)	Correlation length (Å)
$(-\frac{1}{2},3,7)_{\text{off-res.}}$	7.070	215 ± 18
$(-\frac{1}{2},3,7)_{\text{on-res.}}$	7.123	51 ± 3

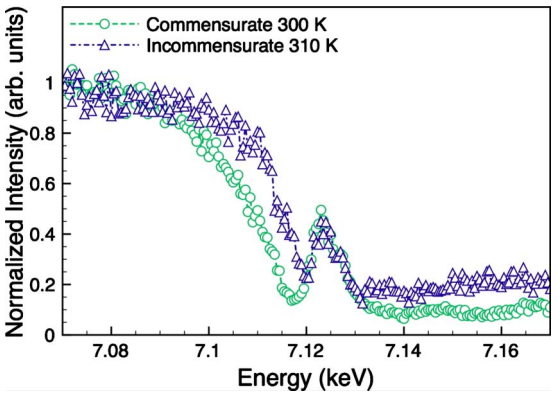

FIG. 7. (Color online) Energy scans of the $(-\frac{1}{2},3,7)$ and $(-\frac{1}{2},3,7+\tau)$ reflections in the σ-σ' channel, measured at fixed wave vector. The spectra have been normalized to the low-energy off-resonance intensities.

deed, if this was the case then BVS calculations could not hope to address questions of charge order. The second option is thus the far more likely. The result is nevertheless surprising, as by any conventional measure several microns deep represents the bulk of the sample.

Energy scans of the reflection were collected during warming, below and above the commensurate-incommensurate transition, $T_{\text{CM-ICM}}$, Fig. 7. There is a change in intensity between the spectra, as is clear from comparison to Fig. 8. However, as will be discussed in Sec. V A, it is the shape of the spectra that explicitly reveals changes to the charge disproportionation. Although the shape of the spectra evolves on warming from 220 to 300 K, there

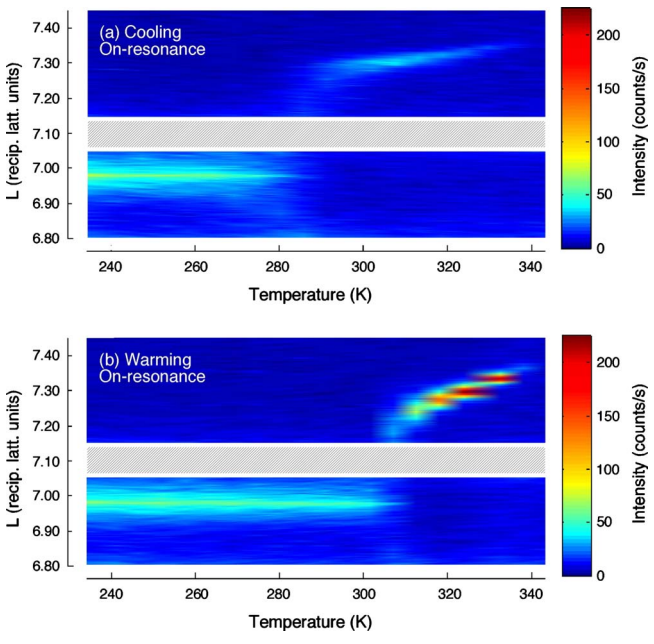

FIG. 8. (Color online) Temperature dependence on (a) cooling and (b) warming of the $(-\frac{1}{2},3,7)$ and $(-\frac{1}{2},3,7+\tau)$ reflections in the σ-σ' channel, measured on-resonance at 7.123 keV [see the marked position in Fig. 5(a)]. The sample was cooled/warmed at a rate of 0.2 K/min. The hashed area contains contamination from a powder reflection.

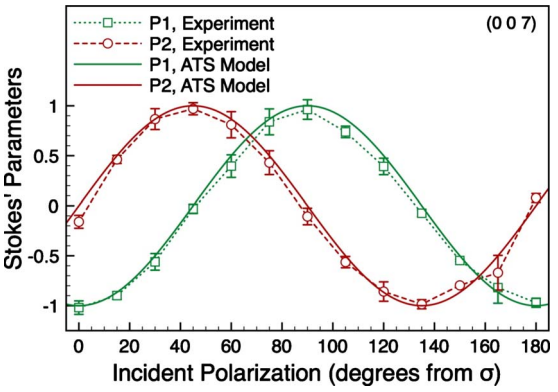

FIG. 9. (Color online) Linear polarization analysis for the (0, 0, 7) reflection, measured at 220 K at 7.122 keV. The solid lines show the behavior expected for an ATS reflection in the high-temperature structure.

are no significant differences in the shape immediately over the transition, indicating there is not any large change to the charge disproportionation upon moving into the incommensurate phase. Such a result is consistent with the interpretation of the CM-ICM transition as being due to the formation of antiphase domain boundaries,[9,29] rather than a fundamental change in the charge structure.

The temperature dependencies measured on cooling and warming are shown in Fig. 8. These results agree well with the temperature dependence measured previously,[9] with T_{CO} at 340 K and $T_{CM\text{-}ICM}$ at 290 K, on cooling. The figure also clearly establishes $T_{CM\text{-}ICM}$ as 310 K on warming. This behavior is consistent with the hysteresis observed in resistivity measurements.[9]

IV. POLARIZATION ANALYSIS

We find that for most of the half-integer reflections studied, the resonant component measured in the σ-π' channel is not simply analyzer leakthrough but contains a component genuinely from this channel. This is made apparent when the differences in the shapes of the spectra between the σ-σ' and σ-π' channels are considered, as seen in Figs. 5(a) and 5(c). To assess this apparent anisotropy, several reflections were subjected to full polarization analysis. The procedure of rotating the polarization of the incident linear light is similar to the more commonplace method of rotating the sample, in that both methods allow any anisotropy to be detected. Isotropic charge scattering is generally the dominant process far from an absorption edge; however, at an edge numerous resonant contributions may be present. These contributions may include a resonant isotropic term, as well as resonant anisotropic terms constrained by the symmetry of the crystal structure; the aforementioned ATS components. The results for the forbidden (0, 0, 7) reflection measured on-resonance are shown in Fig. 9. As anticipated, the reflection shows the expected dependence for an ATS reflection for the high-temperature structure.

To fully characterize the polarization dependence, several charge order reflections were studied both at the resonant energy and at a lower energy, far from the absorption edge.

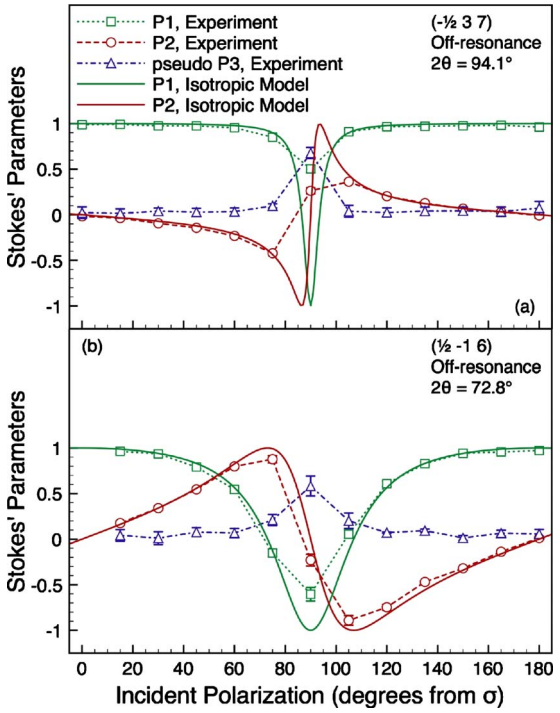

FIG. 10. (Color online) Linear polarization analysis of the (a) $(-\frac{1}{2},3,7)$ and (b) $(\frac{1}{2},-1,6)$ reflections, measured at 220 K, off-resonance. The solid lines show the behavior expected for isotropic charge scattering.

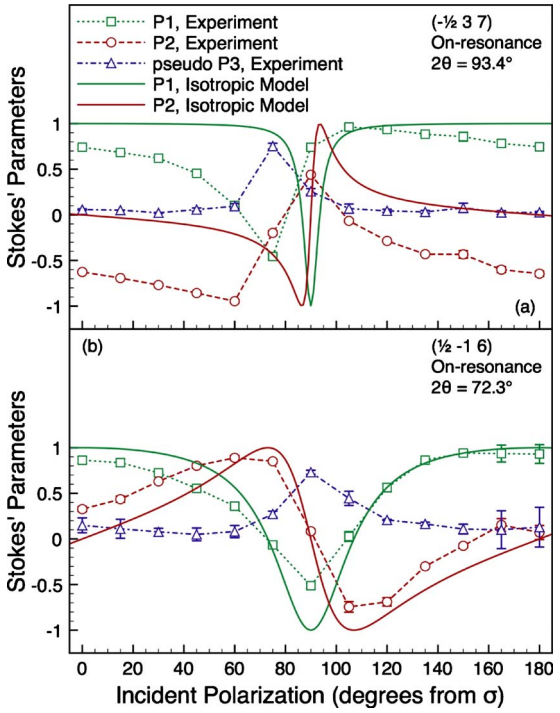

FIG. 11. (Color online) Linear polarization analysis of the (a) $(-\frac{1}{2},3,7)$ and (b) $(\frac{1}{2},-1,6)$ reflections, measured at 220 K, on-resonance. The solid lines show the behavior expected for isotropic charge scattering.

TABLE III. Stokes' parameters for incident circular polarization, measured off-resonance at 7.0812 keV. The expected values for isotropic charge scattering are also shown.

Reflection	Measured P_1	Measured P_2	Isotropic P_1	Isotropic P_2
Main beam	0.008 ± 0.007	-0.042 ± 0.007	0	0
(0, 0, 6)	0.786 ± 0.057	-0.056 ± 0.047	0.777	0
$(-\frac{1}{2},3,7)$	0.955 ± 0.022	-0.046 ± 0.017	0.989	0

TABLE IV. Stokes' parameters for incident circular polarization, measured on-resonance at 7.1227 keV. The expected values for isotropic charge scattering are also shown.

Reflection	Measured P_1	Measured P_2	Isotropic P_1	Isotropic P_2
Main beam	0.009 ± 0.004	-0.050 ± 0.004	0	0
(0, 0, 6)	0.688 ± 0.087	-0.008 ± 0.073	0.787	0
$(-\frac{1}{2},3,7)$	0.772 ± 0.054	-0.544 ± 0.050	0.993	0

The results using linearly polarized light can be seen in Figs. 10 and 11. Figure 10 confirms that the off-resonant reflections are entirely isotropic. Similarly, Fig. 11(b) confirms that the resonant $(\frac{1}{2},-1,6)$ reflection was similarly isotropic and the small σ-π' component was negligible. Meanwhile Fig. 11(a) for the $(-\frac{1}{2},3,7)$ reflection displays very different behavior, including a large nonlinearly polarized component for an incident polarization of 75°. It is important to point out that while this nonlinearly polarized component at 75° is real, the nonlinearly polarized components seen in Figs. 10(a), 10(b), and 11(b) at 90° (π channel) are not. Due to the sample geometry, all of the reflections surveyed were at high 2θ angles. As the intensity in the π-π' channel has a $\cos^2(2\theta)$ dependence for isotropic scattering, the genuine intensity is very low when 2θ is close to 90°, and thus a systematic error is introduced into the measurement.

The same analysis was also carried out for the $(\frac{1}{2},0,6)$ reflection, which possessed an almost identical dependence to the $(\frac{1}{2},-1,6)$ reflection shown in Figs. 10(b) and 11(b). Polarization analysis was carried out for the $(-\frac{3}{2},2,6)$ reflection on-resonance only, which demonstrated the same atypical nonlinearly polarized component at 75° as the $(-\frac{1}{2},3,7)$ reflection. The deviation from isotropic behavior for the $(-\frac{3}{2},2,6)$ is of a similar magnitude to the $(-\frac{1}{2},3,7)$, and shows an almost identical dependence, and hence is not shown.

Data were also collected on the (0, 0, 6) Bragg reflection and the $(-\frac{1}{2},3,7)$ reflection, using circularly polarized incident light. The measured Stokes' parameters are given in Tables III and IV, as are the expected values for isotropic charge scattering. For incident circular polarization, which is composed of σ and π light, 90° out of phase, we expect that scattering close to a 2θ value of 90° will reduce the π' component significantly for isotropic charge scattering. In this case we see that below the resonant energy we obtain exactly the result that we expect. However, on-resonance we find that the scattered light from the $(-\frac{1}{2},3,7)$ reflection is displaced away from the σ' plane.

V. ANALYSIS AND DISCUSSION

To address the question of charge ordering, the *ab initio*, cluster-based, monoelectronic FDMNES code[30] was employed. FDMNES is able to generate the Thomson (f_0) and resonant scattering factors (f' and f'') from an input crystal structure and atom specific charge configuration. The simulations were performed using multiple-scattering mode, with a 6 Å cluster radius containing approximately 91 atoms. The charge disproportionation was simulated in FDMNES by specifying the electronic configuration of each unique site. Only the E1-E1 excitation channel was included as the E1-E2 and E2-E2 components were found to be negligible. Unfortunately, due to the nanoscale domain twinning problem present within the crystal, producing a definitive low-temperature crystal structure has proved unfeasible. Indeed, within such a system the idea of a single-crystal structure starts to become unrealistic. The spectra can be very sensitive to the structure as well as the charge disproportionation, and so without a highly accurate structure all of the predicted spectra are unlikely to simultaneously fit the experimental data. However, we can still obtain compelling results regarding the physics of the system.

The crystal structure obtained from previous x-ray diffraction experiments is an average over two oppositely distorted charge ordered structures, and so is not correct for either individual structure. In order to proceed we have thus applied the diagonal and zigzag structures obtained from GGA+U calculations.[9] An initial implementation of the FDMNES code using these structures, with full ($1e^-$) and with no ($0e^-$) charge disproportionation revealed some interesting results. When comparing to the observed reflections, we found that although most of the spectra did not fit well for any individual model, the diagonal model was successful in predicting the existence of all the reflections and resonant enhancements. Indeed many of the resonant features were found to exist even in the absence of charge order. Specifically, resonances in the rotated σ-π' channel were routinely observed in the absence of charge order while in the σ-σ' channel resonant features were sometimes present but typically small. Meanwhile the zigzag structure incorrectly predicted the existence/absence of several reflections and resonant enhancements, confirming that such a configuration is incorrect.

A. Charge disproportionation

In proceeding only the diagonal structure was implemented. The simulations using this structure revealed that while some spectra were only weakly sensitive to charge order, and some only experienced minor changes in shape with/without charge disproportionation, other reflections experienced much larger changes. Specifically, the presence of any resonant enhancement was found to be almost entirely due to the charge disproportionation for the $(\frac{1}{2},0,6)$, $(-\frac{1}{2},4,7)$, $(\frac{1}{2},-1,7)$, $(-\frac{1}{2},3,7)$, and $(-\frac{3}{2},1,6)$ reflections. For

these reflections it became apparent that the size of the charge disproportionation is related to the relative size of the resonant feature in the σ-σ' channel, with large disproportionations producing a more pronounced resonant enhancement. It is thus important to recognize that the temperature dependence performed on-resonance for the $(-\frac{1}{2},3,7)$ reflection is a reliable study of the charge order.

Of the five spectra whose resonances demonstrated a large dependence on the charge order, four were selected for use in estimating the charge disproportionation. The two formally Fe^{3+} ions were constrained to have equal valences, and were allowed to vary between $Fe^{2.5+}$ and Fe^{3+}, while the formally Fe^{2+} ions were also constrained together and allowed to vary between Fe^{2+} and $Fe^{2.5+}$, simultaneous to the Fe^{3+} ions. The results of the simulations are shown in Fig. 12. In all cases the intensities have been normalized to the off-resonant components, and the energy is calibrated using a fluorescence measurement. Here we can see that while the full $1e^-$ disproportionation typically overestimates the resonant contribution, removing the charge order underestimates it. Applying a charge disproportionation of $0.4e^-$ produces a reasonable fit but still underestimates the resonance in most cases. Allowing the program to vary the charge order results in the best fit for a disproportionation of $0.74e^-$. It is clear that the fitted spectra do not perfectly match the experimental spectra, as the ratio between the resonant and nonresonant features is not exact, and in all cases the higher energy shoulder is over estimated; however, there is clearly some agreement between simulation and experiment. The key features are replicated, and only in the case of the $(-\frac{3}{2},1,6)$ reflection is the resonant enhancement over estimated. As a result we are unable to determine an exact charge disproportionation between the formally Fe^{2+} and Fe^{3+} sites. However, we are able to estimate the lower and upper bounds of the disproportionation as $0.4e^-$ and $0.8e^-$. Thus RXD suggests that Fe_2OBO_3 has an unusually large charge disproportionation which is crucial to the presence of the surprisingly strong charge order energy resonances.

While the estimated disproportionation is considerably larger than the majority of similar compounds, determined via the same method, our result seems to contradict the conclusion of integer valence states deduced by BVS analysis.[12] It appears that there are two distinct causes for this discrepancy. As previously discussed, since the correlation length appears to be shorter within the first 5 μm, it is possible that there may be a difference of the charge disproportionation between this region and the bulk. Such a difference would contribute to the contradiction between studies, as the spectra we observe is representative of a combination of both regions. However, any such difference between the charge disproportionation in both regions is likely to be small, and so can only partially explain the inconsistency. BVS analysis is an empirical method which is dependent on the intimate connection between local geometry/bond lengths and ion valence states. It is a *fingerprint method* that relies on comparison with known nonmixed-valence reference compounds. In the FDMNES simulations, the electronic configuration is specified (without recalculating the structure), and the above estimated charge disproportionation is therefore a quantity distinct from the separation of valence states deduced to be close to integer in Ref. 12. Given that even nonmixed-valence compounds such as Fe_2O_3 have no integer charge on the Fe ions due to hybridization with oxygen, it is perhaps not surprising that the difference in orbital occupation is less than the difference in empirical valence.

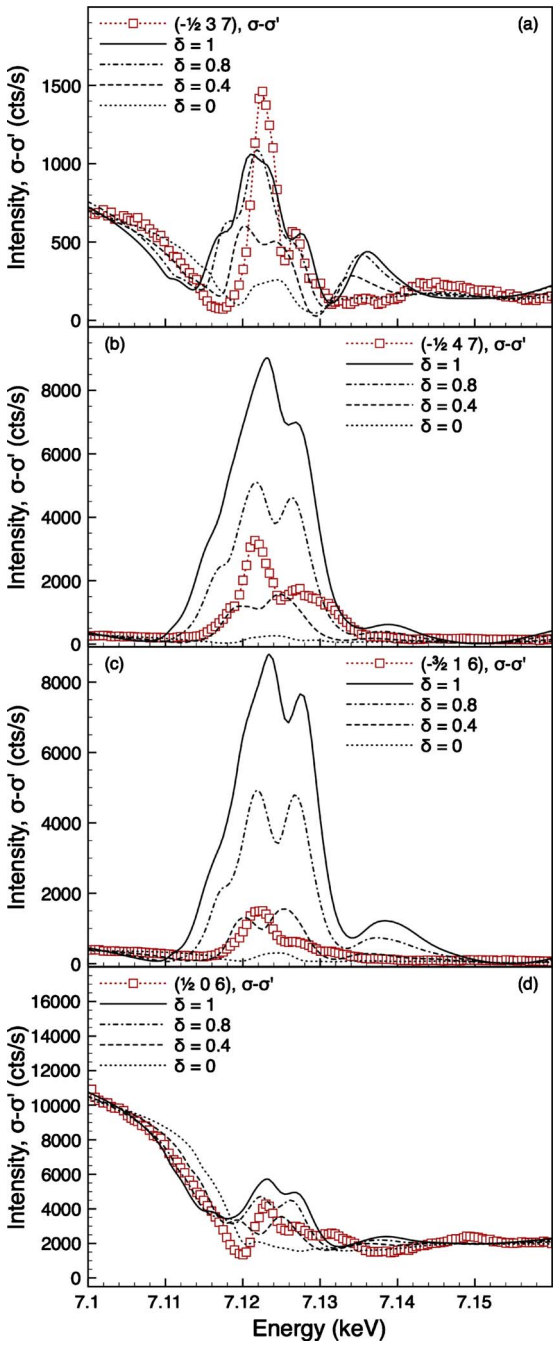

FIG. 12. (Color online) Experimental spectra and simulations at 220 K, of the (a) $(-\frac{1}{2},3,7)$, (b) $(-\frac{1}{2},4,7)$, (c) $(-\frac{3}{2},1,6)$, and (d) $(\frac{1}{2},0,6)$ reflections, showing the effect of charge disproportionation on the resonance. The simulations use the diagonal structure and apply iron valences of $+2.5\pm\frac{\delta}{2}$. The simulation has been corrected to include absorption.

Due to the increased widths of the reflections on resonance, some of the resonant intensity is surely missed in the energy scans. Such an effect could be compensated by col-

lecting the energy spectra in the form of rocking curves at separate energies, and then extracting the integrated intensity; however, such a study is far more time consuming, and so was not possible in this case. The effect of our use of peak values rather than integrated intensities is an underestimation of the actual resonant enhancement, meaning that the charge disproportion could be slightly larger than that deduced here.

B. Polarization effects

We have found that off-resonance all of the reflections demonstrate a clear isotropic charge scattering dependence, Fig. 10. This is exactly what we expect for scattering from the scalar Thomson (isotropic nonresonant) terms. We have found that for the majority of reflections, isotropic scattering still provides an excellent description of the measured dependence at the resonant energies. This is not surprising, as on-resonance we expect the dominant terms to be the isotropic resonant components, along with a Thomson contribution. However, as already described, the contribution in the σ-π' channel is often larger than expected for isotropic scattering, even though this contribution is generally very small. For the $(-\frac{3}{2},2,6)$ and $(-\frac{1}{2},3,7)$ reflections deviations are seen from the isotropic behavior. However, it is only when studying the $(-\frac{1}{2},3,7)$ reflection, where the polarization dependencies at and below the resonant energy are compared using both linearly and circularly polarized light, that such a difference can be fully appreciated. Why is it that such atypical behavior is seen for these two reflections and not the others surveyed? Although all of the reflections surveyed have 2θ values approaching 90°, the specific reflections in question have $2\theta \approx 90°$ and so the isotropic scattering components are highly attenuated in the π' scattered channel, allowing the anisotropic terms to be observed. Simulations using the FDMNES code using a charge disproportionation of $0.74e^-$ produce a good agreement with the observed result, as shown in Fig. 13(a). Figure 14 confirms that the charge ordered structure closely replicates the measured nonlinearly polarized contribution. Interestingly, Fig. 13(b) reveals that such an effect is not reliant on the charge disproportionation, although in this case the simulation including charge disproportionation clearly produces a better agreement.

A substantial change to the nonlinearly polarized contribution occurs when the nonresonant component is excluded from the simulation, suggesting that the interference between the Thomson terms and E1-E1 resonant terms may have the dominant role in performing the polarization conversion. However, inspection of the contributions from each of the individual components (Thomson, resonant isotropic and resonant anisotropic) reveals that the Thomson and resonant isotropic terms have approximately the same magnitude at the relevant energy of 7.1227 keV in all polarization channels. We also find that the dominant contributions in orthogonal polarization channels come from the isotropic terms in one channel and the anisotropic terms in the other, thus revealing that it is the interference between the isotropic and anisotropic terms which is responsible for the production of nonlinearly polarized light.

A similar polarization conversion has previously been reported in K_2CrO_4,[20] where the conversion resulted from interference between the E1-E1 and E2-E2 scattering channels at a forbidden reflection. Such a conversion was also observed in magnetite,[21] as a result of interference between E1-E1 components from different iron sublattices. The mechanism responsible for the phenomenon in iron oxyborate is thus subtly different and may be used to explain similar observations at allowed reflections in other materials.

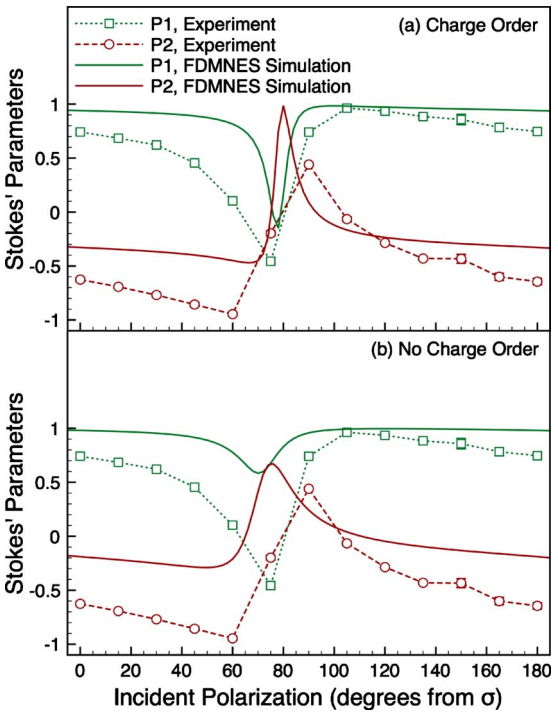

FIG. 13. (Color online) Comparison between the experimental and simulated polarization dependencies for the $(-\frac{1}{2},3,7)$ reflection (a) with and (b) without charge ordering, with both simulations at 7.1227 keV (on-resonance).

VI. CONCLUSIONS

In this comprehensive RXD study of Fe_2OBO_3 at the iron K edge a number of important results have become apparent.

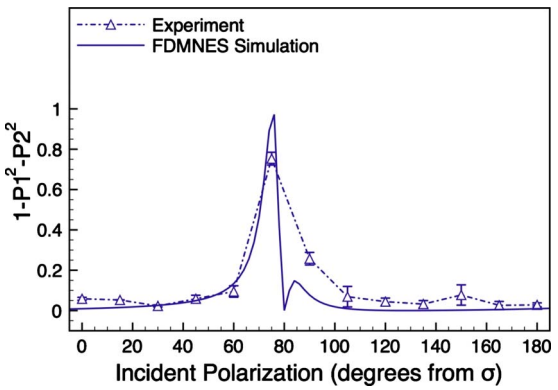

FIG. 14. (Color online) Charge ordered FDMNES simulation of the pseudo-P_3 component for the $(-\frac{1}{2},3,7)$ reflection, on-resonance at 7.1227 keV.

Before this analysis it was clear that there were numerous effects associated with the rate of warming and cooling: namely, the *freezing in* of incommensurate reflections and the hysteretic nature of the resistivity. Here, we have demonstrated the hysteresis of a resonant enhancement almost entirely associated with the charge order. We have also observed the development of slightly incommensurate reflections within the formally commensurate phase, which eventually condense into commensurate reflections. We have found no significant changes to the spectra immediately over $T_{\text{CM-ICM}}$, indicating there is not any large change to the charge structure on moving into the incommensurate phase. Such a result is consistent with the formation of antiphase domain boundaries as an explanation for the CM-ICM transition.[9,29]

Using simulations generated by the FDMNES code we have confirmed that the zigzag structure cannot be the correct ground state while the diagonal structure can be used to qualitatively simulate all results. Although we have been unable to assign an accurate value to the charge segregation, we are able to estimate the disproportionation as being between $0.4e^-$ and $0.8e^-$. Thus we have demonstrated that despite some previous reports to the contrary,[31] Fe_2OBO_3 is indeed charge ordered, but that the differences between the $3d$ electronic configuration of inequivalent sites is noninteger. We have demonstrated that under certain conditions we can observe a nonlinearly polarized component to the scattered beam from linearly polarized incident light, and confirmed this conversion using incident circularly polarized light. Through simulations we find that the effect appears to primarily result from interference between isotropic and anisotropic scattering components.

We are unable to replicate the spectra exactly due to the problems surrounding the exact low-temperature crystal structure, specifically the nanoscale domain structure, however our results replicate the key features. This is the first resonant x-ray diffraction study of iron oxyborate, which is a comparatively understudied material. Once a more appropriate structure can be determined, the data contained herein may be re-examined to more exactly determine the charge disproportionation.

ACKNOWLEDGMENTS

The authors wish to thank the ESRF for the beamtime and experimental support. S.R.B., R.D.J., and P.D.H. thank EPSRC and STFC for funding. M.A. and S.A. acknowledge support by the Initiative and Networking Fund of the Helmholtz Association of German Research Centers through the Helmholtz-University Young Investigator Group Complex Ordering Phenomena in Multifunctional Oxides and by the institute of scattering methods. S.R.B. thanks Y. Joly for helpful discussions and assistance with FDMNES, and C. B. Buckley for additional experimental support. The authors thank R. P. Hermann for preliminary measurements and helpful EXAFS discussions and results. This work was partially performed on the EPSRC-funded XMaS beamline at the ESRF, directed by M. J. Cooper and C. A. Lucas. We are grateful to the beamline team of S. D. Brown, P. Normile, O. Bikondoa, L. Bouchenoire, and P. Thompson for their invaluable assistance, and to S. Beaufoy and J. Kervin for additional support.

[1] E. Wigner, Phys. Rev. **46**, 1002 (1934).
[2] J. Kanamori, J. Appl. Phys. **31**, 14S (1960).
[3] K. I. Kugel', Sov. Phys. Usp. **25**, 231 (1982).
[4] J. B. Goodenough, Phys. Rev. **100**, 564 (1955).
[5] S. Mori, C. H. Chen, and S.-W. Cheong, Nature (London) **392**, 473 (1998).
[6] P. G. Radaelli, D. E. Cox, L. Capogna, S.-W. Cheong, and M. Marezio, Phys. Rev. B **59**, 14440 (1999).
[7] J. P. Attfield, A. M. T. Bell, L. M. Rodriguez-Martinez, J. M. Greneche, R. J. Cernik, J. F. Clarke, and D. A. Perkins, Nature (London) **396**, 655 (1998).
[8] J. P. Attfield, A. M. T. Bell, L. M. Rodriguez-Martinez, J. M. Greneche, R. Retoux, M. Leblanc, R. J. Cernik, J. F. Clarke, and D. A. Perkins, J. Mater. Chem. **9**, 205 (1999).
[9] M. Angst, R. P. Hermann, W. Schweika, J.-W. Kim, P. Khalifah, H. J. Xiang, M.-H. Whangbo, D.-H. Kim, B. C. Sales, and D. Mandrus, Phys. Rev. Lett. **99**, 256402 (2007).
[10] J. P. Attfield, J. F. Clarke, and D. A. Perkins, Physica B **180-181**, 581 (1992).
[11] I. Leonov, A. N. Yaresko, V. N. Antonov, J. P. Attfield, and V. I. Anisimov, Phys. Rev. B **72**, 014407 (2005).
[12] M. Angst, P. Khalifah, R. P. Hermann, H. J. Xiang, M.-H. Whangbo, V. Varadarajan, J. W. Brill, B. C. Sales, and D. Mandrus, Phys. Rev. Lett. **99**, 086403 (2007).
[13] P. M. Woodward, D. E. Cox, T. Vogt, C. N. R. Rao, and A. K. Cheetham, Chem. Mater. **11**, 3528 (1999).
[14] J. García, M. Concepción Sánchez, J. Blasco, G. Subías, and M. G. Proietti, J. Phys.: Condens. Matter **13**, 3243 (2001).
[15] R. J. Goff and J. P. Attfield, Phys. Rev. B **70**, 140404(R) (2004).
[16] E. Nazarenko, J. E. Lorenzo, Y. Joly, J. L. Hodeau, D. Mannix, and C. Marin, Phys. Rev. Lett. **97**, 056403 (2006).
[17] G. Subías, J. García, P. Beran, M. Nevřiva, M. Concepción Sánchez, and J. L. García-Muñoz, Phys. Rev. B **73**, 205107 (2006).
[18] J. Herrero-Martín, G. Subías, J. García, J. Blasco, and M. Concepción Sánchez, Phys. Rev. B **79**, 045121 (2009).
[19] R. D. Johnson, S. R. Bland, C. Mazzoli, T. A. W. Beale, C.-H. Du, C. Detlefs, S. B. Wilkins, and P. D. Hatton, Phys. Rev. B **78**, 104407 (2008).
[20] C. Mazzoli, S. B. Wilkins, S. DiMatteo, B. Detlefs, C. Detlefs, V. Scagnoli, L. Paolasini, and P. Ghigna, Phys. Rev. B **76**, 195118 (2007).
[21] S. R. Bland, B. Detlefs, S. B. Wilkins, T. A. W. Beale, C. Mazzoli, Y. Joly, P. D. Hatton, J. E. Lorenzo, and V. A. M. Brabers, J. Phys.: Condens. Matter **21**, 485601 (2009).
[22] L. Paolasini *et al.*, J. Synchrotron Radiat. **14**, 301 (2007).
[23] S. D. Brown *et al.*, J. Synchrotron Radiat. **8**, 1172 (2001).
[24] V. Scagnoli, C. Mazzoli, C. Detlefs, P. Bernard, A. Fonacaro, L.

Paolasini, F. Fabrizi, and F. de Bergevin, J. Synchrotron Radiat. **16**, 778 (2009).
[25] E. Hecht, *Optics*, 4th ed. (Addison-Wesley, Reading, MA, 2002).
[26] V. E. Dmitrienko, Acta Crystallogr., Sect. A: Found. Crystallogr. **39**, 29 (1983).
[27] D. H. Templeton and L. K. Templeton, Phys. Rev. B **49**, 14850 (1994).
[28] M. Renninger, Z. Phys. **106**, 141 (1937).
[29] Y. J. Song, H. X. Yang, H. F. Tian, C. Ma, Y. B. Qin, L. J. Zeng, H. L. Shi, J. B. Lu, and J. Q. Li, Phys. Rev. B **81**, 020101(R) (2010).
[30] Y. Joly, Phys. Rev. B **63**, 125120 (2001).
[31] J. García and G. Subías, Phys. Rev. B **74**, 176401 (2006).